Variable-temperature NMR investigation into the fluxional thermodynamics of metallocene-containing cryptands

C. Dennis Hall, and Nelson W. Sharpe

Organometallics, **1990**, 9 (4), 952-959• DOI: 10.1021/om00118a009 • Publication Date (Web): 01 May 2002

the solution chromatographed on silica gel. Elution with dichloromethane–hexane, increasing the proportion of CH_2Cl_2 from 1:20 to 1:4, to 1:2.3, and finally to 1:1, removed in sequence maroon, dark-green, green, and dark-red bands. The first eluate afforded **7a** (0.035 g, 12%), and the dark-green fraction, after removal of solvent, gave **7b** (0.05 g, 17%). The green eluate yielded dark-green microcrystals of **7c** (0.03 g, 10%), and the dark-red eluate gave 0.06 g of $\{CpFe(CO)_2\}_2$.

7c: IR ν_{max}(CO) 2067 s, 2016 s, 1984 s, and 1860 s cm^{-1} (hexane); mass spectrum, m/e 498 (M^+), other peaks, $M^+ - x$(CO) (x = 1–4), 292 (M – 4CO – FeF_2), 198 (M – 4CO – $2FeF_2$).

Thermal Transformation of Complexes [Cp(CO)Fe(μ-C(CF$_3$)=C(CF$_3$)SMe)Fe(CO)$_3$] (7a and 7c) to [(CpFe)$_2$(μ-CO)$_2$(μ-C(CF$_3$)≡C(CF$_3$))] (8). Approximately 0.15 g of **7a** was heated in toluene at reflux for 3 h, affording a dark-violet solution. The solvent was removed in vacuo, the residue was extracted with dichloromethane, and the extracts were chromatographed on silica gel. Elution with dichloromethane–hexane (1:9) removed a violet band, which was evaporated to yield product **8** (0.05 g, 72%).

Similarly, **7c** heated in toluene at reflux for 24 h gave mostly **8** with traces of **7a** and **7b** (^{1}H NMR analysis).

8: Anal. Calcd for $C_{16}H_{10}F_6Fe_2O_2$: C, 41.8; H, 2.2. Found: C, 41.6; H, 2.3. IR ν_{max}(CO) 1803 s, ν(CC) 1600 m cm^{-1} (CH_2Cl_2); mass spectrum, m/e 460 (M^+), other peaks, 432 (M – CO), 404 (M – 2CO), 261 (M – 2CO – C_4F_5).

Isomerization Experiments. The reaction was performed in a sealed glass tube (volume 3 cm^3) containing cluster **6** (2 mg, 3.3×10^{-6} mol), along with the 1-hexene (0.4 cm^3, 3.2×10^{-3} mol) to be isomerized; the tube was filled with nitrogen by standard vacuum techniques. The reaction was conducted at 132 °C for 1.5 h, and at this stage about 32% of 1-hexene had been isomerized. The isomerization solutions were examined by ^{1}H and ^{13}C NMR spectroscopy to reveal the extent of isomerized hexene. The organic products in solution after isomerization experiments were analyzed by GLC (PPG/Chromosorb-W).

Crystal Structure of {Fe(CO)$_3$}$_2${μ-(CF$_3$)CCC[Fe(η^5-C$_5$H$_5$)(CO)$_2$]} (5). The specimen was a red plate 0.84 × 0.72 × 0.36 mm. All measurements were made at 22 °C on an Enraf-Nonius CAD4F diffractometer using Mo Kα X-rays, λ = 0.71069 Å, monochromated by reflection from a graphite crystal.

Crystal data: $C_{17}H_5F_3Fe_3O_8$, M_r = 561.8, orthorhombic, space group $Pbca$, a = 13.533 (4), b = 14.748 (4), c = 20.067 (3) Å^3, U = 4005 (2) Å^3, Z = 8, D_{calcd} = 1.863 g cm^{-3}, F(000) = 2208, μ(Mo Kα) = 22.1 cm^{-1}.

Cell dimensions were determined from the setting angles of 23 reflections with $13 \le \theta(\text{Mo K}\alpha) \le 17°$, and the space group from the systematic absences. The intensities of 9694 reflections (h $\bar{19}$ to 19, k $\bar{7}$ to 20, l $\bar{9}$ to 28) with $2 \le \theta(\text{Mo K}\alpha) \le 30°$ were determined from $\omega/2\theta$ scans of 0.90° in ω. Correction for Lp and absorption effects (relative transmission factors on F 0.75–1.22) and averaging (R_{int} = 0.035) yielded 5790 unique intensities, of which 2619 with $I \ge 3\sigma(I)$ were subsequently used.

The iron atoms were located from a sharpened Patterson synthesis, and the remaining atoms from difference syntheses. In the final full-matrix least-squares minimization of $\sum w(|F_o| - |F_c|)^2$ with $w^{-1} = \sigma^2(F) + 0.0004F^2$ the positions and anisotropic displacement parameters of all non-hydrogen atoms were refined. Hydrogen atoms were constrained to ride on the carbon atoms to which they were attached, with C–H = 0.96 Å and U(H) ≃ 1.2U(C). The refinement converged ($\Delta/\sigma < 0.08$ with R = 0.041 and R_w = 0.055). Final [$\Delta\rho$] values did not exceed 0.63 e Å^{-3}. Neutral atom scattering factors and complex anomalous dispersion corrections were taken from ref 26. Calculations were performed on a Gould 3227 computer with the GX package.[27] Final atomic coordinates are listed in Table III (supplementary material).

Acknowledgment. The CNRS, Brest University (R.R. and F.P.), and Glasgow University and SERC (Lj.M.-M. and K.W.M.) are acknowledged for financial support. We are grateful to Dr. R. Pichon (Brest) for assistance in NMR experiments and to Dr. D. Picard for recording some mass spectra.

Registry No. 1, 104730-97-4; 2, 118773-68-5; 3, 125051-03-8; 4, 118772-53-5; 5, 125051-04-9; 6a, 118772-52-4; 6b, 125076-47-3; 7a, 125076-46-2; 7b, 125051-06-1; 7c, 125134-35-2; 8, 125051-05-0; $Fe_3(CO)_{12}$, 17685-52-8; Fe, 7439-89-6; 1-hexene, 592-41-6; *cis*-2-hexene, 7688-21-3; *trans*-2-hexene, 4050-45-7; *cis*-3-hexene, 7642-09-3; *trans*-3-hexene, 13269-52-8.

Supplementary Material Available: Tables of fractional atomic coordinates and isotropic and anisotropic displacement parameters and a complete bond length and angle listing for **5** (4 pages); a listing of observed and calculated structure factors for **5** (12 pages). Ordering information is given on any current masthead page.

(27) Mallinson, P. R.; Muir, K. W. *J. Appl. Crystallogr.* **1985**, *18*, 51.

Variable-Temperature NMR Investigation into the Fluxional Thermodynamics of Metallocene-Containing Cryptands

C. Dennis Hall* and Nelson W. Sharpe

Department of Chemistry, King's College, University of London, Strand, London, U.K. WC2R 2LS

Received June 14, 1989

Variable-temperature ^{13}C and ^{1}H 2D COSY and ^{13}C–^{1}H shift correlation spectra have been used to determine the solution structure of 1,1′-(1,4,10,13-tetraoxa-7,16-diazacyclooctadecane-7,16-diyldicarbonyl)ferrocene and its ruthenium homologue together with the thermodynamic parameters for rotation of the amide carbonyl group in both molecules. Consideration of the ^{13}C NMR spectra allows a correlation to be established between the shielding effects and the metallocene-centered molecular orbital structure of these molecules.

Introduction

Metallocene-containing cryptands are attractive as redox-active host molecules for selective recognition and binding of cations.[1-8] To assess the potential for interactive phenomena between two proximally disposed metal centers, it is important to appreciate the dynamics of

(1) Akabori, S.; Habata, Y.; Sakamoto, Y.; Sato, M.; Ebine, S. *Bull. Chem. Soc. Jpn.* **1983**, *56*, 537.

(2) Beer, P. D. *J. Chem. Soc., Chem. Commun.* **1985**, 1115.

(3) Saji, T.; Kinoshita, I. *J. Chem. Soc., Chem. Commun.* **1986**, 716.

(4) Beer, P. D.; Crane, C. G.; Keefe, A. D.; Whyman, A. R. *J. Organomet. Chem.* **1986**, *314*, C9.

(5) Saji, T. *Chem. Lett.* **1986**, 275.

0276-7333/90/2309-0952$02.50/0

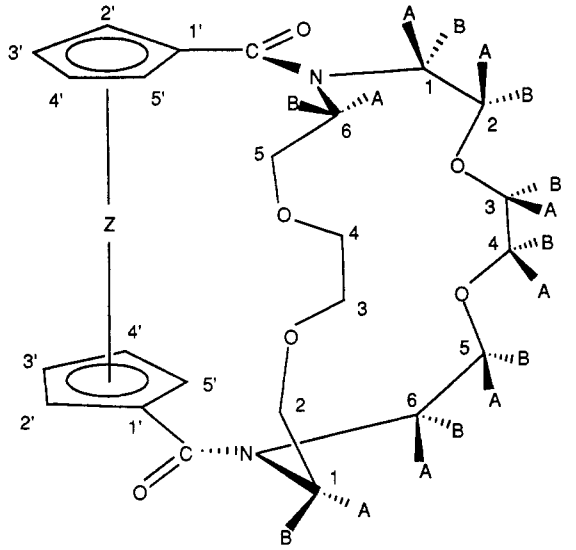

Figure 1. Stereochemical representation of 1,1′-(1,4,10,13-tetraoxa-7,16-diazacyclooctadecane-7,16-diyldicarbonyl)metallocene, together with atom identification nomenclature (A and B are hydrogen atoms). Compound **1**, Z = Fe, and compound **2**, Z = Ru. Note, ring numbering is consistent with Figure 11 in ref 9.

molecular fluxionality in the polydentate framework of the coordinating metallocene-containing macrocycle. In this paper, we report the total ^1H and ^{13}C NMR analysis of the Fe and Ru homologues of the metallocene cryptand, depicted in Figure 1. This has proved possible by the use of the 2D COSY and ^{13}C–^1H shift correlation techniques. We also report the kinetics associated with the intramolecular fluxional dynamics for each homologue as derived from variable-temperature NMR studies. These parameters are discussed with respect to their relative molecular freedoms in terms of the inter-ring dimensions and the macrocyclic bridging unit. Detailed consideration of the NMR shifts of the metallocene ring nuclei allow a refined model for the electronic molecular orbital description of the metallocene moiety to be deduced.

These studies aid design strategies of host molecules. The thermodynamic parameters associated with the conformational changes required for complexation determine the equilibria for host–guest interaction and illustrate the factors influencing the transition state leading to complex formation. Detailed NMR experiments permit analysis of solution structures, essential for the study of complexes since these have not been isolated in a crystalline form suitable for X-ray analysis. Finally, an understanding of the perturbation of molecular orbital levels within the host cryptand affords an indication of the energetics that may control electron transfer within host–guest complexes.

Experimental Section

Compound **1** was synthesised and purified in the manner reported earlier,[9] as was compound **2** according to an identical method from ruthenocene dicarbonyl chloride as starting material. Both gave satisfactory elemental analyses and relative molecular masses by mass spectrometry. Both are in fact isolated as dihyrates, the ruthenocenyl cryptand tending to effloresce with ease. For the NMR studies reported here, the dihydrates were used, since they are highly soluble and stable in toluene as solvent. Toluene-d_8 was used as supplied by Aldrich, and the NMR spectra were recorded on a Bruker WH 360-MHz spectrometer, with the temperature probe calibrated against ethylene glycol as standard.

Table I. ^{13}C and ^1H Chemical Shifts for the Metallocene Cryptand Nuclei in Toluene-d_8 as Solvent (in ppm Relative to Internal TMS; ^1H δ Values Refer to Multiplet Centroids)

^{13}C			^1H		
nucleus	1	2	nucleus	1	2
C=O	170.01	168.68			
C-1′	79.37	84.55			
C-2′	73.92	75.58	H-2′	4.87	5.31
C-3′	71.89	71.90[a]	H-3′	4.19	4.40
C-4′	73.47	73.85	H-4′	4.43	4.61
C-5′	70.78	74.95	H-5′	4.63	4.94
C-1	50.39	49.14	H-1A	2.40	2.51
			H-1B	4.06[b]	4.13
C-2	69.39	70.90[c]	H-2A	2.99	3.09[b]
			H-2B	4.07[b]	3.89
C-3	70.44	70.90[c]	H-3A, H-3B	3.35 (2)[d]	3.33 (1)
C-4	73.38	71.90[a]	H-4A, H-4B	3.25 (2)	3.20–3.30 (3)
C-5	70.50	70.31	H-5A	3.53	3.39[b]
			H-5B	3.90	3.54
C-6	51.43	51.32	H-6A	2.76	3.15[b]
			H-6B	4.02[b]	4.02

[a] Separated by DEPT. [b] Multiplets overlap. [c] Do in fact resolve at elevated temperatures. [d] Refers to number of protons under this resonance.

Results and Discussion

Assignment of NMR Spectra. The full listing of both ^{13}C and ^1H chemical shift data for compounds **1** and **2** are presented in Table I. The ^{13}C assignment for the ferrocenyl cryptand, **1**, is in agreement with that previously reported[9] for the same compound in $CDCl_3$ as solvent. It has been refined since C-3′ and C-4′ have been unambiguously identified. The ^{13}C assignments for **2**, the ruthenocenyl cryptand, have been reported earlier[10] for $CDCl_3$ as solvent. These have been found in error and have been reassigned in this paper correctly. These improvements in spectra assignment have been made possible by considering the 2D COSY and ^{13}C–^1H shift correlation spectra for the respective compounds.

For compound **1**, Figures 2 and 3 show the 2D COSY and ^{13}C–^1H shift correlation spectra, respectively. That four resonance signals only are associated with the eight ring protons is consistent with the C_2 axis of symmetry for the molecule (in solution on the NMR time scale), whose structure in the solid state has recently been determined by X-ray crystallography.[11] With respect to the ring protons, the 2D COSY spectrum indicates that the ^1H resonance at 4.87 ppm couples strongly with that at 4.19 ppm while more weakly with those at 4.43 and 4.63 ppm, and that the ^1H resonance at 4.63 ppm couples strongly with that at 4.43 ppm while more weakly with those at 4.87 and 4.19 ppm. Thus, the resonances at 4.87 and 4.63 ppm are associated with the protons H-2′ and H-5′. It remains only to identify one of the four proton signals for the other three to be assigned as well. Inspection of the X-ray crystal structure indicates that it is the H-2′ proton that resides in the deshielding zone of the conical anisotropic shielding associated with the carbonyl group, i.e., it is coplanar and cis. This identifies the resonance that is most deshielded

(6) Andrews, M. P.; Blackburn, C.; McAleer, J. F.; Patel, V. D. *J. Chem. Soc., Chem. Commun.* **1987**, 1122.
(7) Beer, P. D.; Sikanyika, H.; Blackburn, C.; McAleer, J. F. *J. Organomet. Chem.* **1988**, *350*, C15.
(8) Hall, C. D.; Sharpe, N. W.; Danks, I. P.; Sang, Y. P. *J. Chem. Soc., Chem. Commun.* **1989**, 419.
(9) Hammond, P. J.; Bell, A. P.; Hall, C. D. *J. Chem. Soc., Perkin Trans. I* **1983**, 707.
(10) Beer, P. D.; Elliot, J.; Hammond, P. J.; Dudman, C.; Hall, C. D. *J. Organomet. Chem.* **1984**, *263*, C37.
(11) Beer, P. D.; Bush, C. D.; Hamor, T. A. *J. Organomet. Chem.* **1988**, *339*, 133.

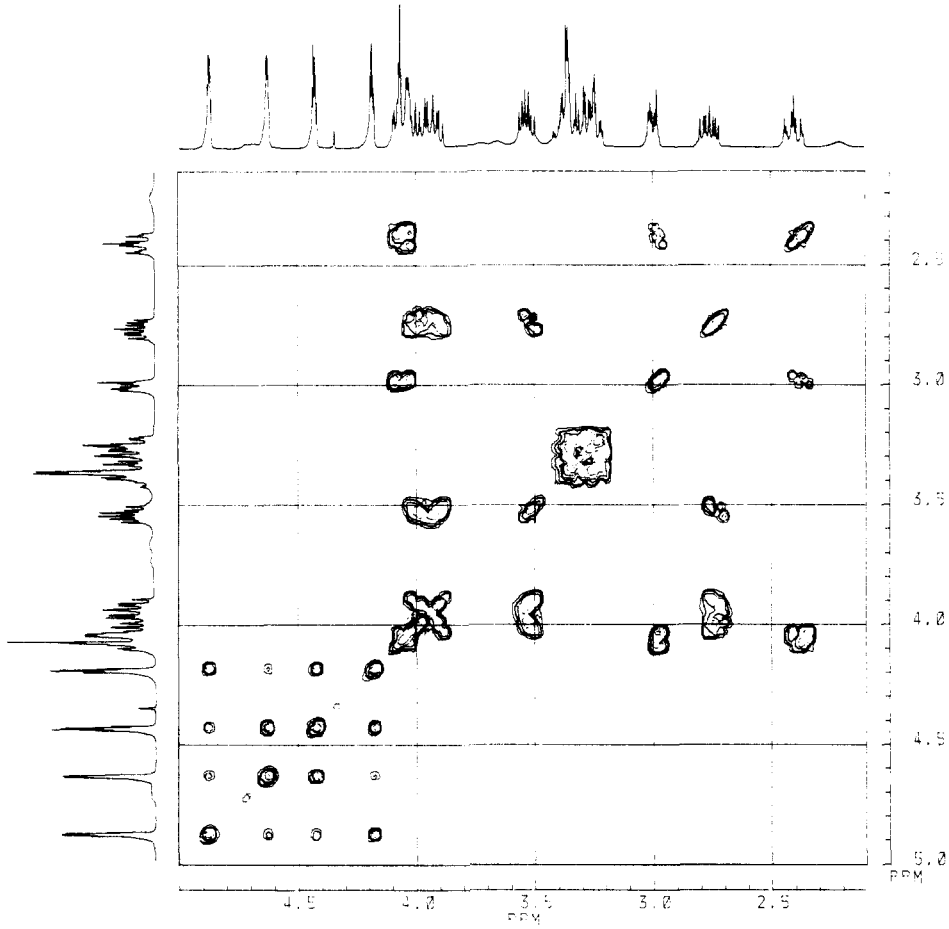

Figure 2. 2D COSY spectrum of 1.

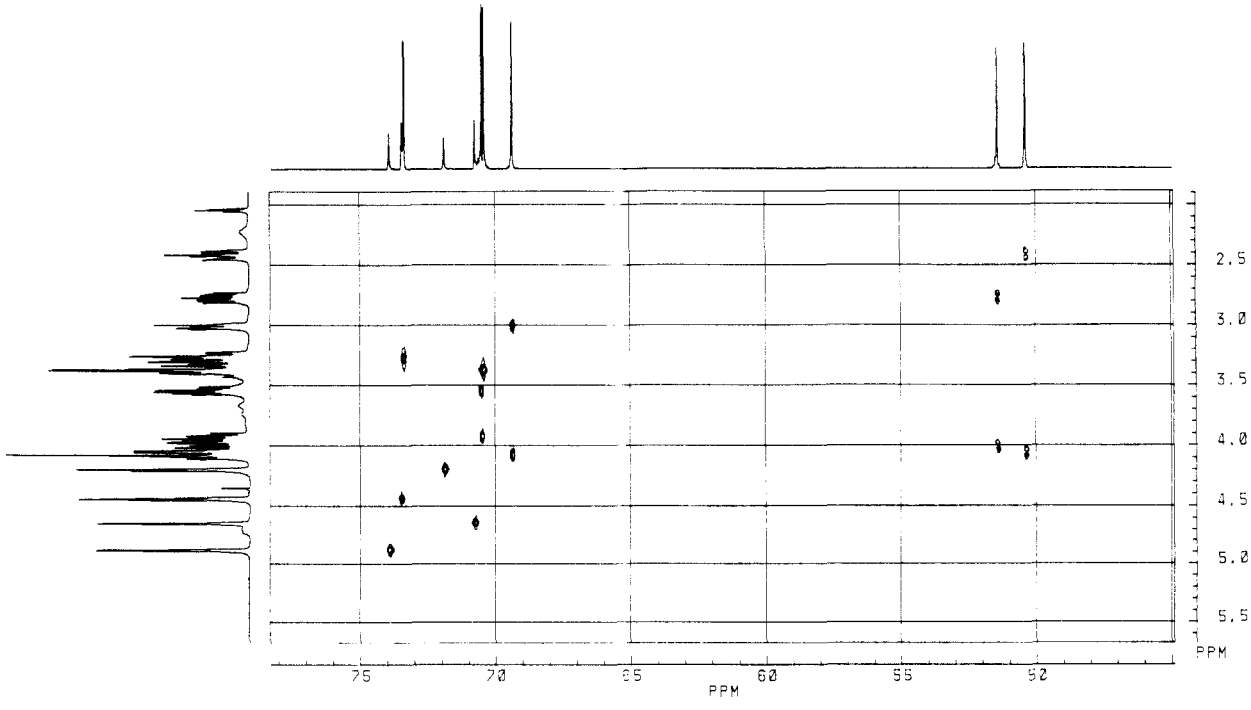

Figure 3. $^{13}C-^{1}H$ shift correlation spectrum of 1.

as that for H-2′, i.e., that at 4.87 ppm, and as such affords assignment for all the other ring resonances. Examination of the 2D COSY shows that the signal at 4.19 ppm must be due to H-3′ (two strong couplings, one to H-2′), the signal at 4.43 ppm must be due to H-4′ (two strong couplings), and that at 4.63 ppm must be due to H-5′ (one strong coupling with H-4′). As required by the analysis, the signals at 4.87 and 4.63 ppm (H-2′, H-5′) coalesce to their midpoint on heating, as do the signals at 4.19 and 4.43 ppm (H-3′, H-4′). The dynamic process responsible is rotation of the amide carbonyl group, which affords equivalence in the magnetic environments of the proton

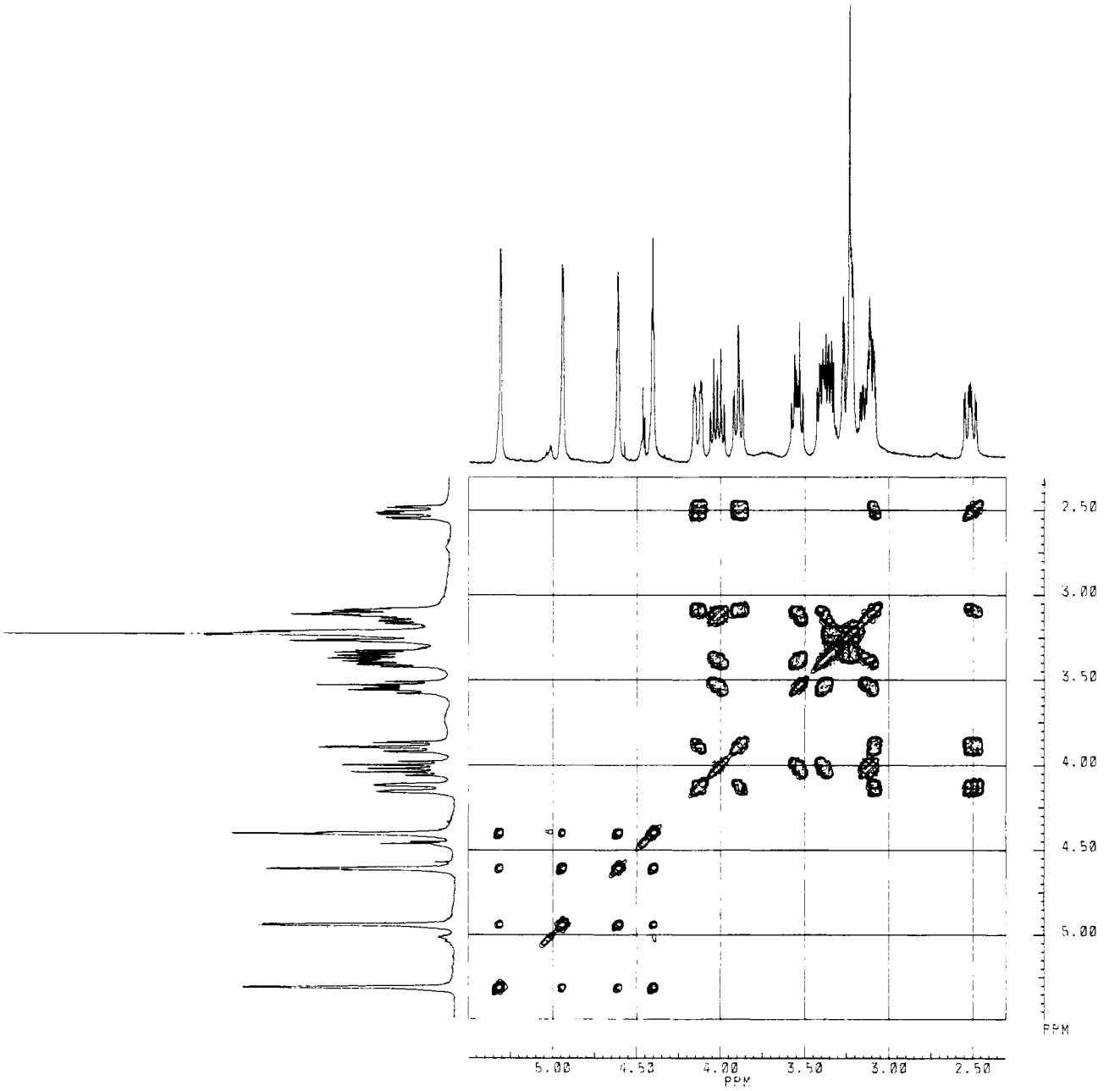

Figure 4. 2D COSY spectrum of **2**.

pairs. Given this assignment of ring protons, the ^{13}C–^{1}H shift correlation spectrum (Figure 3) permits the umambiguous identification of the resonances for the five ring carbon magnetic environments for **1**.

By reference to earlier studies on dialkylamides[12-15] we are able to assign the higher field NCH_2 ^{13}C resonance at 50.39 ppm to C-1, i.e., that which is cis to the amide carbonyl group. The ^{13}C–^{1}H shift correlation spectrum shows that the two proton resonances associated with nuclei directly bonded to C-1 occur as multiplets centered on 2.40 and 4.06 ppm. The X-ray crystal structure indicates that it is nucleus H-1B that resides in the carbonyl deshielding zone, and therefore H-1B may be assigned as 4.06 ppm and H-1A as the signal at 2.40 ppm. The resonance at 2.76 ppm is seen to coalesce with H-1A to their midpoint at elevated temperature (387 K). It is therefore identified as H-6A, which becomes magnetically equivalent to H-1A when amide carbonyl roation is rapid on the NMR time scale. Having identified H-1A, the 2D COSY permits identification of the pair H-2A and H-2B and the ^{13}C–^{1}H shift correlation spectrum the identity of C-2. Likewise assigning H-6A identifies H-6B and the pair H-5A and H-5B and thus the C-6 and C-5 carbons. For the pairs H-2A, H-2B and H-5A, H-5B, reference to the X-ray crystal structure once more indicates which of each is the more deshielded by spatial disposition relative to the amide carbonyl.

No method enables us to distinguish between the ^{13}C resonances associated with C-3 and C-4 at 70.44 and 73.38 ppm or allows us to distinguish the protons H-3A, H-3B, H-4A, and H-4B, whose multiplets resonate as a cluster in the region 3.2–3.4 ppm. The 2D COSY and ^{13}C–^{1}H shift correlation spectra, however, are consistent with these assignments.

For the ruthenocenyl derivative, **2**, the corresponding 2D COSY and ^{13}C–^{1}H shift correlation spectra are repro-

(12) Paulsen, H.; Todt, K. *Chem. Ber.* **1967**, *100*, 3385.
(13) Liden, A.; Roussel, C.; Liljefors, T.; Chanon, M.; Carter, R. E.; Metzger, J.; Sandstrom, J. *J. Am. Chem. Soc.* **1976**, *98*, 2853.
(14) Jones, R. G.; Wilkins, J. M. *Org. Magn. Reson.* **1978**, *11*, 20.
(15) Fritz, H.; Hug, P.; Sauter, H.; Winkler, T.; Lawesson, S.-O.; Pederson, B.; Scheibye, S. *Org. Magn. Reson.* **1981**, *16*, 36.

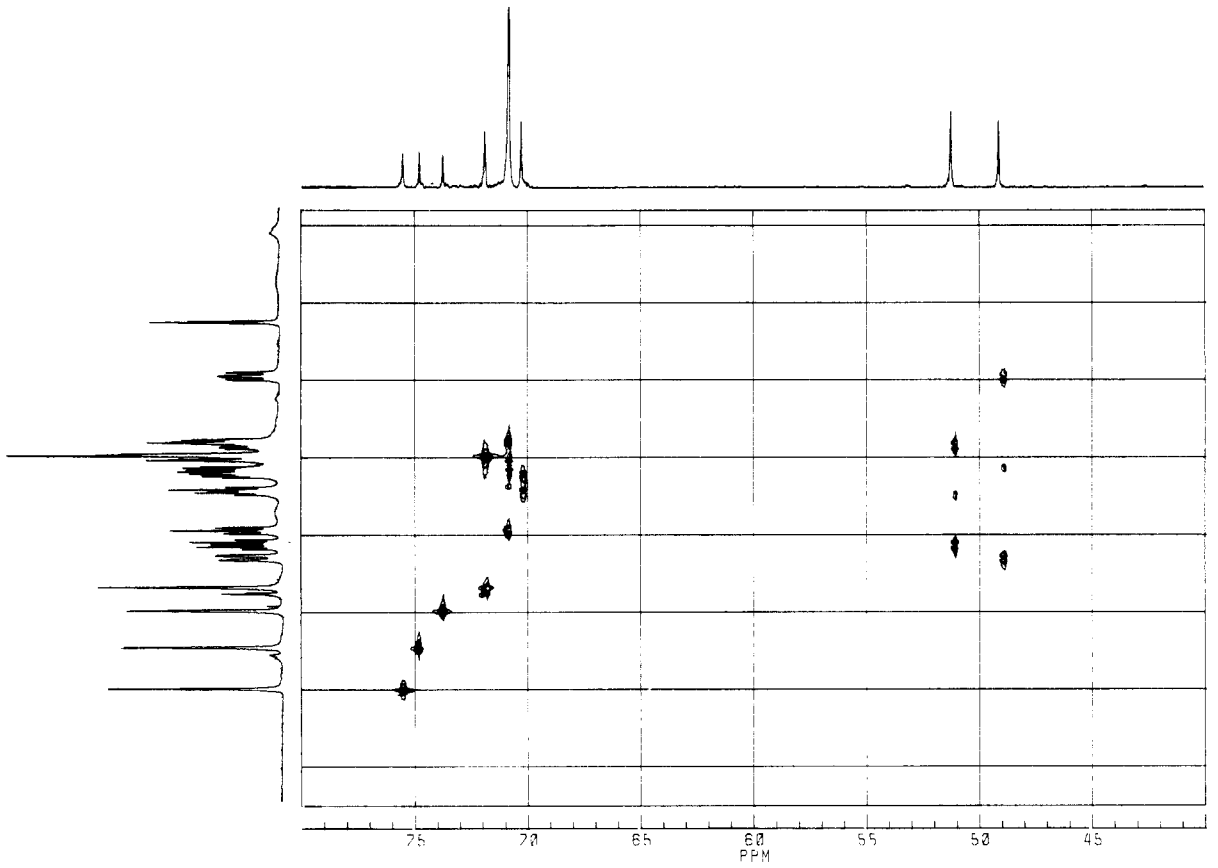

Figure 5. $^{13}C-^{1}H$ shift correlation spectrum of **2**.

duced in Figures 4 and 5 respectively. The same methodology as described for **1** above permits the assignments presented in Table I for **2** with equal validity. As observed in **1** and likewise for **2**, only four resonances for the cyclopentadienyl ring protons are evident, consistent with a C_2 axis of symmetry. These assignments are also consistent with the variable-temperature coalescence pairs (detailed later) observed at elevated temperatures for rotation of the amide carbonyl group as the dynamic process, identical with the processes observed with **1**. The variation in chemical shift for each nucleus from one homologue to the other leads us to conclude that the ruthenocenyl derivative is broadly isostructural with the ferrocenyl homologue. The X-ray crystal structure for the ferrocenyl derivative, **1**, shows that the N---N distance is 5.220 Å compared with 5.843 Å for the N---N distance in the parent diaza crown, which results in puckering of the polyether chains. In contrast, for the ruthenocenyl derivative, given an interplanar distance between the cyclopentadienyl rings of ca. 3.68 Å[16,17] (as compared to 3.286 Å for **1**) the calculated N---N distance yields a value of ca. 5.73 Å for **2** with concomitant unpuckering of the ring. This accounts for the changes in chemical shift for the methylenic nuclei, both ^{13}C and ^{1}H, in going from one homologue to the other. Worthy of greater consideration is the observation that for both homologues the ordering of the cyclopentadiene ring proton chemical shifts (from lower to higher field) is H-2′ > H-5′ > H-4′ > H-3′. In the ^{13}C spectra, however, this ordering is C-1′ > C-2′ > C-5′ > C-4′ > C-3′ for the ruthenocenyl but C-1′ > C-2′ > C-4′ > C-3′ > C-5′ for the ferrocenyl derivative. This counterintuitive observation may also be rationalized upon the basis that the homologues are isostructural with respect to their metallocene conformation.

(16) Seiler, P.; Dunitz, J. D. *Acta Crystallogr.* **1982**, *B38*, 1741.
(17) Hardgrove, G. L.; Templeton, D. H. *Acta Crystallogr.* **1959**, *12*, 28.

Table II. Coalescence Temperature (T_c), Chemical Shift Differences ($\Delta\nu$), and Rate Coefficients at Coalescence (k_c) from the ^{1}H and ^{13}C NMR Spectra for 2 (Toluene-d_8 as Solvent)

nuclei pair[a]	T_c, K	$\Delta\nu$, Hz	k_c,[b] s^{-1}
H-1B,H-6B	353 (±2.5)	41.5	92.2
H-3′,H-4′	359 (±2)	73.8	164.0
C-2′,C5′	364.5 (±2.5)	56.2	124.8
C-3,C-4	371.5 (±3.5)	91.6	203.6
H-2′,H-5′	374 (±1.5)	132.8	295.0
H-2B,H-5B	376 (±3.5)	126.1	280.3
H-1A,H-6A	380 (±3.5)	229.4	509.8
C-3′,C-4′	382 (±5)	176.8	392.7
C-1,C-6	385 (±5)	199.2	442.7

[a] C-2,C-5 pair coalesces at less than 60 °C; H-5A,H-2A pair coalesces, but T_c impossible to estimate. [b] $k_c = \pi\Delta\nu/(2^{1/2})$.

Variable-Temperature Studies. The ruthenocenyl cryptand, **2**, is seen to exhibit fluxional behavior on the NMR time scale at elevated temperature. The mechanism is rotation of the amide carbonyl through a transition state in which the carbonyl π bond is orthogonal to the ground-state planar π-bonding framework constituted by the cyclopentadienyl–amide system. This transition state may be closely similar to that required for complexation of metal cations in which the carbonyl groups become cis (details to be reported later). Since the molecule possesses a C_2 axis of symmetry, this leads to equivalence of the magnetic environment of pairs of ^{1}H and ^{13}C nuclei. The coalescence temperatures (T_c) for several pairs of nuclei are given in Table II together with the calculated values of the rate coefficients at coalescence (k_c). In each case coalescence to the resonance midpoint is observed. From these data we are able to calculate the various thermodynamic parameters for the amide carbonyl rotation.

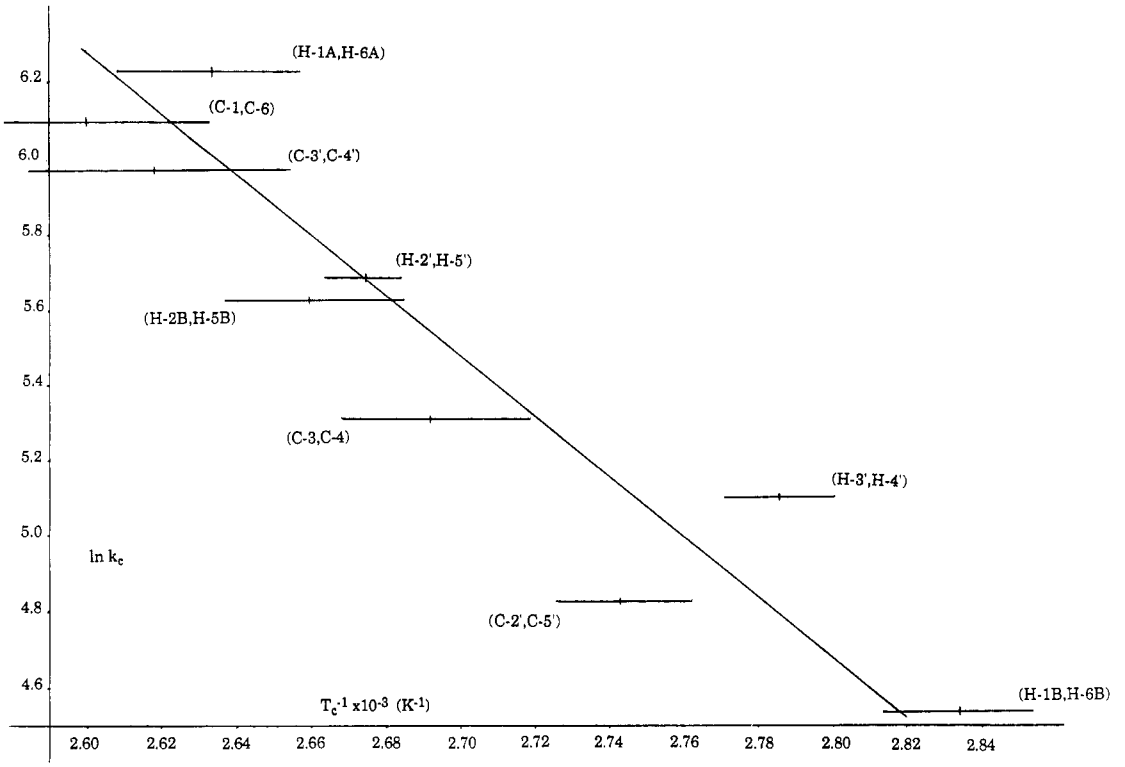

Figure 6. Arrhenius plot of log k_c versus $1/T_c$ for the coalescence events of **2** (see also Table II).

Table III. Activation Parameters for the Coalescence Phenomena Observed in the ^{1}H and ^{13}C NMR Spectra for the Family of Metallocene Cryptands[a]

		373 K				298 K	
compd	E_a, kcal mol^{-1}	k_c, s^{-1}	$\Delta G^{\ddagger}$, kcal mol^{-1}	$\Delta H^{\ddagger}$, kcal mol^{-1}	$\Delta S^{\ddagger}$, kcal mol^{-1}	k_c, s^{-1}	$\Delta G^{\ddagger}$, kcal mol^{-1}
2							
Z = Ru, $m = n = 2$	15.9 (±1.6)	278	17.8	15.2 (±1.6)	−6.9 (±3)	1.4 (±0.7)	17.2
1							
Z = Fe, $m = n = 2$		195	18.1				
Z = Fe, $m = 2$, $n = 1$	12.4 (±1.1)	4171	15.8	11.6	−11.2 (±2)	62	15.1
Z = Fe, $m = 3$, $n = 2$	11.0 (±1.5)	2385	16.2	10.3	−16.03 (±3)	57	15.1
Z = Fe, $m = 3$, $n = 3$	8.5 (±1.6)	985	16.9	7.8	−24.5 (±3)	55	15.0

[a] Data for the additional three ferrocenyl derivatives from ref 18, in which m and n define the number of oxygen atoms in each polyether chain of the parent diazacrown.

Figure 6 shows the Arrhenius plot for these data, from which E_a, the experimentally determined activation energy for the carbonyl rotation, was derived. Upon cooling, both the original room-temperature ^{13}C and ^{1}H NMR spectra are regenerated, and therefore no decomposition has occurred. Errors are largely in $1/T_c$, since the precision in determining the exact coalescence event is inherently ±1 K, particularly if the coalescence occurs in a region close to other resonance signals.

In contrast to earlier reports from this laboratory,[10] coalescence features were observed for **1** at the highest temperatures in toluene-d_8. At ca. 387 K, the resonances associated with the protons H-1A and H-6A ($\Delta\nu$ = 129.0 Hz) and those with the ^{13}C nuclei C-1 and C-6 ($\Delta\nu$ = 94.2 Hz) are clearly seen to coalesce to their midpoints; the accuracy of the temperature calibration at this high temperature is however less reliable. At 373 K (±1.5 K) the ring proton resonances associated with H-2′ and H-5′ ($\Delta\nu$ = 87.6 Hz) and H-3′ and H-4′ ($\Delta\nu$ = 87.9 Hz) are also seen to coalesce to their midpoint. Hence for the ferrocenyl derivative, $\Delta G^{\ddagger}$ at 373 K is 18.1 kcal mol^{-1}, whereas for the ruthenocenyl derivative $\Delta G^{\ddagger}$ at 373 K is 17.8 kcal mol^{-1}. The lower value for the free energy of activation for carbonyl bond rotation in **2** reflects both a less rigid and less strained molecular framework owing to the greater interplane dimension of ruthenocene and the concomitant unpuckering of the cryptand ring for the ruthenocenyl cryptand. Since both E_a and $\Delta G^{\ddagger}$ are available for the ruthenocenyl cryptand, **2**, we can calculate values of $\Delta H^{\ddagger}$ and $\Delta S^{\ddagger}$, which are presented in Table III together with those calculated for similar ferrocene cryptands from data reported earlier.[18]

Table III shows that the entropy of activation for the dynamic process is least for the ruthenocenyl derivative. This implies that the increase in the degree of order during reorganization of the molecule to the transition state is least for the ruthenocenyl derivative. This again reflects the greater inter-ring distance. Amongst the ferrocenyl derivatives the value of $-\Delta S^{\ddagger}$ increases with the number of atoms enjoined in this reorganization. The values of $\Delta H^{\ddagger}$ reflect the extent to which the ground state is stabilized with respect to the transition state. In the transition state the carbonyl π-bonding framework is orthogonal to the ground-state ring amide coplanar π-bonding framework. It is therefore evident that the ruthenocenyl derivative possesses a ground-state configuration in which the ring amide π-bonding framework is most coplanar (i.e.,

(18) Hammond, P. J.; Beer, P. D.; Dudman, C.; Danks, I. P.; Hall, C. D.; Knychala, J.; Grossel, M. C. *J. Organomet. Chem.* **1986**, *306*, 367.

Table IV. Ring ^{13}C Chemical Shifts for 1 and 2 in ppm Relative to Internal TMS in Toluene-d_8

nucleus	1	2	Δ, additional deshielding for nucleus in 2, ppm
C-1′	79.37	84.55	+5.18
C-2′	73.92	75.58	+1.66
C-3′	71.89	71.90	+0.01
C-4′	73.47	73.85	+0.38
C-5′	70.78	74.94	+4.16

least distorted). This confirms the NMR chemical shift evidence for unpuckering of the cryptand ring as a consequence of increased N---N distance, which in turn alleviates stress at the carbonyl.

For the ferrocenyl derivative our only reliable values are for k_c and $\Delta G^{\ddagger}$ at 373 K. Lack of further coalescence values below the boiling point of toluene precludes construction of an Arrhenius plot. The value of $\Delta G^{\ddagger}$ is greatest for **1**, reflecting the greater rigidity of the compound relative to other ferrocene cryptands. In general, however, the thermodynamic data confirm that **1** and **2** possess similar structures.

Electronic and Molecular Orbital Structure. As remarked earlier, the ordering of deshielded ring protons (from lower to higher field) for both the ruthenocenyl and ferrocenyl derivatives is the same, namely, H-2′ > H-5′ > H-4′ > H-3′. However, in the ^{13}C spectra the ordering of deshielded ^{13}C nuclei for the ruthenocenyl derivative is C-1′ > C-2′ > C-5′ > C-4′ > C-3′ but C-1′ > C-2′ > C-4′ > C-3′ > C-5′ for the ferrocenyl derivative. Table IV collects together these ^{13}C shifts and shows the *relative* increase in deshielding (in ppm) in going from the ferrocenyl to the ruthenocenyl derivative. These apparently disparate trends may be rationalized in terms of the bonding within these molecules, as follows.

For the proton resonances, the chemical shift of each ^1H nucleus is determined by the through-bond and through-space interactions. Through bond interactions relate to the σ- and π-bonding framework within, principally, the cyclopentadienyl amido ligand. Through-space interactions relate to the spatial disposition of the nuclei relative to other functional groups, predominantly, the conical anisotropic shielding about the carbonyl group. For broadly isostructural compounds in solution, these parameters for both the ruthenocenyl and the ferrocenyl derivatives are similar, and as such the ordering of deshielded ring protons for each is identical.

However, for the ^{13}C nuclei, the metal–carbon bonding interaction and the bonding electron density about the ^{13}C nucleus (the electronic factor) influence the shielding afforded to each individual ^{13}C nucleus. For d^6 metallocenes in the eclipsed conformation (D_{5h} symmetry) the five metal-centered d orbitals split to span the molecular orbitals a_1', e_2', and e_1'', as shown by Zerner et al.[19] Of these the a_1' (d_{z^2}) and the e_2' (d_{xy}, $d_{x^2-y^2}$) molecular orbitals are bonding, and the e_1'' (d_{xz}, d_{yz}) antibonding through interaction with the ligand orbitals. The X-ray crystal structure for **1** indicates that the carbonyl groups on each cyclopentadienyl ring are disposed trans. Furthermore the ipso (C-1′) carbons are one carbon out of step. This is illustrated schematically in Figure 7a, which shows the consequent ring numbering sequence for both upper and lower ring system in relation to the C_2 axis of symmetry. In Figure 7a the bonding metal-centered d_{xy} orbital (for x and y axes defined as shown) is superimposed upon the

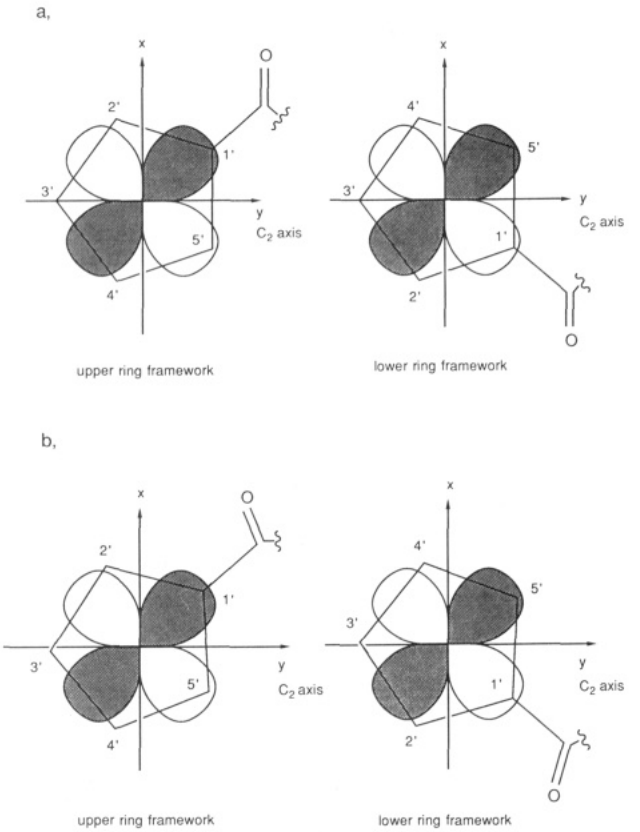

Figure 7. Schematic representation of the interactional overlap of the d_{xy} metal-centered orbital with the ligand-centered orbitals composed pricipally of the carbon-centered $2p_z$ orbitals for a, both upper and lower rings, and b, for the upper and lower rings with twist angle from eclipsed.

illustrated ligand frameworks, the one above and the other below the central metal nucleus at the coordinate origin. It is clear that for the bonding d_{xy} metal-centered orbital, the bonding interaction with the ligand orbitals (i.e., orbital overlap) is maximized in the vicinity of the pair of nuclei C-1′ and C-5′ most, then the pair C-2′ and C-4′, and then least at C-3′. (Note, consideration of the $d_{x^2-y^2}$ orbital produces the ordering C-3′ > C-4′, C-2′ > C-5′,C-1′, i.e., the reverse.) In the case of the ferrocenyl derivative we are considering 3d orbitals, but for the ruthenocenyl derivative 4d orbitals. In the latter, the orbitals are larger and more diffuse, and as such the d_{xy}–ligand orbital interactions illustrated in Figure 7a (which are bonding) necessarily implicate lowered electron densities about the ^{13}C. Hence the cyclopentadienyl ring nuclei in **2** are generally more deshielded than the same nuclei in **1** (Table I). Further, the X-ray crystal structure for **1** indicates that the upper and lower rings as illustrated in Figure 7a are staggered with twist angle 6.4° placing the carbonyl functions at greater separation while maintaining the selfsame C_2 axis of rotation as illustrated in Figure 7b and common to Figure 7a. In **1**, therefore, the metallocene moiety is removed by 6.4° from *local* D_{5h} symmetry. For symmetries lower than D_{5h} the degeneracy of the e_2' and the e_1'' molecular orbitals is lifted. In Figure 7b, the consequence of this twist on the extent of d_{xy}–ligand interaction about the ring carbons is illustrated for the upper and lower ring frameworks. Since the d_{xy} orbital retains its orientation with respect to the C_2 axis and because this axis of symmetry is maintained, the effect on both upper and lower rings is identical. It is clear that this bonding interaction increases somewhat in the vicinity of both C-1′ and C-2′ and somewhat less for C-3′ but decreases some-

(19) Zerner, M. C.; Loew, G. H.; Kirchner, R. F.; Mueller-Westerhoff, U. T. *J. Am. Chem. Soc.* **1980**, *102*, 589.

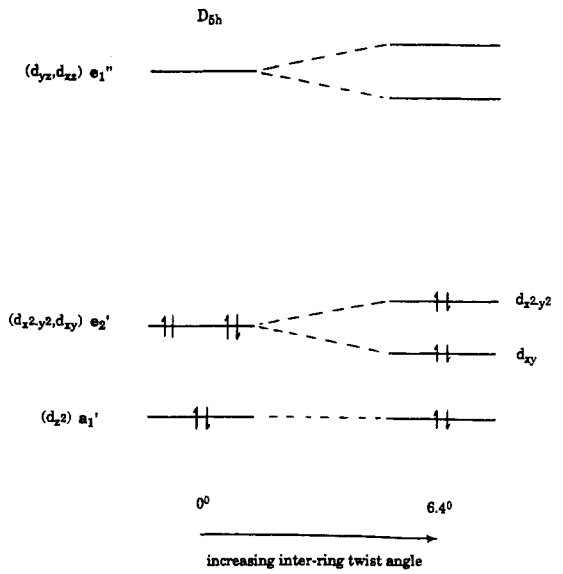

Figure 8. Schematic molecular orbital energy level diagram showing the lifting of metal-centered orbital degeneracies as the inter-ring twist angle increases, thereby lowering the metallocene symmetry from eclipsed (local D_{5h}).

what for C-4′ and C-5′, (again treatment of the $d_{x^2-y^2}$ orbital interactions yields the reverse orderings.) Therefore the extent of the d_{xy}–ligand interactions in **1** and **2** (assuming the two are isostructural) places electron density in the vicinity of the ^{13}C ring nuclei in the order C-1′ > C-5′ ≫ C-2′ > C-4′ ≫ C-3′. Since this interaction is bonding, the *decrease* in electron density about each ^{13}C nucleus for the 4d metallocene, **2**, compared with **1**, which involves less diffuse 3d orbitals, would follow the same order. Therefore in **2**, we expect the *relative* deshielding of resonances compared to those of **1** to be in the order C-1′ > C-5′ ≫ C-2′ > C-4′ ≫ C-3′, and reference to Table IV indicates this to be so. However this argument holds only for consideration of the d_{xy} interaction, and for the $d_{x^2-y^2}$ interaction exactly the reverse trends are anticipated. The experimental NMR shift data may be rationalized as the consequence of twist angle which lifts the degeneracy of the e_2' energies for the exactly eclipsed (local D_{5h}) conformation, and it is the molecular orbital composed principally by the metal-centered d_{xy} orbital that becomes more strongly bonding, as illustrated in Figure 8. Therefore, comparison of the relative chemical shifts for the cyclopentadiene ring carbons for the two homologues in effect utilizes the carbon nuclei as probes for the distribution of electron density within the metallocene framework, which is seen to increase for symmetries lower than D_{5h} in accord with the symmetry associated with the metal-centered d_{xy} orbital.

Acknowledgment. We thank Fran Gallwey for collection of the NMR data and RTZ Chemicals Ltd. for financial support (N.W.S.). We also wish to acknowledge a gift of ruthenium chloride from Johnson Mathey Ltd., which was the source of compound **2**.[18]

Registry No. 1, 71818-07-0; 2, 90385-10-7.

Electrochemical Synthesis and Structure of $Sn[Co(CO)_4]_4$ and Its Use as a Stable Precursor of $[Co(CO)_4]^-$ for the Catalysis of Hydrolysis of Propylene Carbonate

Armando Cabrera,† Henri Samain, André Mortreux, and Francis Petit*

Laboratoire de Chimie Organique Appliquée, URA CNRS 402, ENSC Lille, USTL Flandres Artois, BP 108, 59652 Villeneuve d'Ascq Cédex, France

Alan J. Welch

Department of Chemistry, University of Edinburgh, Edinburgh EH9 3JJ, U.K.

Received June 15, 1989

The complex $Sn[Co(CO)_4]_4$ (I) has been prepared in high yield by the controlled potential electrolysis of $Co_2(CO)_8$ in the presence of a tin anode. The major advantage afforded by this electrochemical synthesis is to produce I quickly and cleanly. Results of an X-ray diffraction study on I are reported. We have established that I and $Co_2(CO)_8$ are very active catalysts for the hydrolysis of cyclic organic carbonates. The 100% selectivity in monoglycol is in marked contrast to other catalytic systems that require an excess of water to inhibit production of polyglycols. Studies, under various CO pressures, of the catalytic activities of $Co_2(CO)_8$ and I during the hydrolysis of propylene carbonate have led us to suggest that (i) $[Co(CO)_4]^-$ is the active moiety, (ii) I can eliminate $Co_2(CO)_8$, and (iii) I is more stable than $Co_2(CO)_8$ at low CO pressures. Isotopic analysis of the remaining substrate and products after the hydrolysis of propylene carbonate by $H_2{}^{18}O$ show that (iv) the attack of water occurs at the carbonyl site of the carbonate and (v) it is likely that hydration is activated by $[Co(CO)_4]^-$.

Introduction

We have recently reported several catalytic systems utilizing electrochemically generated catalysts.[1,2] Electrogeneration of catalysts permits changes in the oxidation state of the metal and gives enhanced possibility of substrate activation. We now report that the complex $Sn[Co(CO)_4]_4$ (I) can be prepared in a pure state and in high yield by controlled-potential electrolysis of $Co_2(CO)_8$ using

† Present address: Instituto di Chimica, Ciudad Universitaria 04150, Mexico.

(1) Mortreux, A.; Petit, F. *J. App. Catal.* **1986**, *24*, 1.
(2) Gilet, M.; Mortreux, A.; Folest, J. C.; Petit, F. *J. Am. Chem. Soc.* **1983**, *105*, 3876.

0276-7333/90/2309-0959$02.50/0